DOI: 10.6060/mhc256828k

New 2D-2D Materials Based on Graphitic Carbon Nitride and MXene for Photocatalytic Applications

Roman F. Alekseev, and Ekaterina A. Kozlova[@]

Boreskov Institute of Catalysis, Siberian Branch of the Russian Academy of Sciences, 630090 Novosibirsk, Russian Federation
[@]Corresponding author E-mail: kozlova@catalysis.ru

Modern society is faced with a pack of interconnected energy and environmental challenges, including rapid fossil fuel exhaustion accompanied by rise of greenhouse gases emissions and contamination of water resources by industrial waste and pharmaceuticals. All of this is aggravated by constantly increasing worldwide energy consumption that makes it economically unfeasible to invest into solving aforementioned problems by traditional means. In such context environmentally safe photocatalytic technologies that rely on sunlight energy are seen as a promising solution. Special attention is paid to composite photocatalysts with synergetic effects such as MXene/g-C_3N_4. These systems have an enhanced photocatalytic activity due to the combination of unique properties of the component: graphitic carbon nitride's excellent visible light absorption and MXene's high electric conductivity and tunable surface properties. The key advantage is formation of an effective 2D-2D interface with improved charge transfer and separation to improve reaction kinetics and charge carrier lifetime. Modern researches are usually aimed at optimization of morphology to achieve close contact between components and to maximize the availability of active sites. This review examines synthetic approaches to creating composite photocatalysts based on g-C_3N_4 and MXene and summarizes data on photocatalyst activity in processes such as hydrogen production, carbon dioxide reduction, and degradation of organic pollutants under light irradiation.

Keywords: Graphitic carbon nitride, MXene, photocatalysis, hydrogen production, carbon dioxide reduction.

Новые 2D-2D материалы на основе графитоподобного нитрида углерода и MXene для фотокаталитических приложений

Р. Ф. Алексеев, Е. А. Козлова[@]

ФИЦ Институт катализа им. Г.К. Борескова СО РАН, 630090 Новосибирск, Российская Федерация
[@]E-mail: kozlova@catalysis.ru

Современное общество сталкивается с комплексом взаимосвязанных энергетических и экологических проблем, включая быстрое истощение запасов ископаемого топлива, сопровождающееся ростом выбросов парниковых газов и загрязнение водных ресурсов промышленными отходами и фармацевтическими препаратами. Все это усугубляется постоянно растущим мировым потреблением энергии, что делает экономически нецелесообразным инвестирование в решение этих проблем традиционными способами. В этом контексте экологически безопасные фотокаталитические технологии, использующие энергию солнечного света, рассматриваются как перспективное решение. Особое внимание уделяется композитным фотокатализаторам с синергетическим эффектом, таким как MXene/g-C_3N_4. Эти системы обладают повышенной фотокаталитической активностью благодаря сочетанию уникальных свойств компонентов: превосходного поглощения видимого света графитоподобным нитридом углерода и высокой электропроводности и регулируемых свойств поверхности MXene. Ключевым преимуществом является формирование эффективного 2D-2D интерфейса с улучшенным переносом и разделением заряда для улучшения кинетики реакции и увеличения времени жизни носителей заряда. Современные исследования, как правило, направлены на оптимизацию морфологии для достижения

плотного контакта между компонентами и максимальной доступности активных центров. В данном обзоре рассмотрены синтетические подходы к созданию композитных фотокатализаторов на основе g-C_3N_4 и MXene, а также суммированы данные по активности фотокатализаторов в таких процессах как получение водорода, восстановление углекислого газа и разрушение органических загрязнителей под действием света.

Ключевые слова: Графитоподобный нитрид углерода, MXene, фотокатализ, получение водорода, восстановление углекислого газа.

Introduction

The global energy crisis and environmental problems define the increasing significance of photocatalytic technologies in modern science.[1,2] Continued growth of fossil energy resources consumption is accompanied by a number of critical problems, including increase of greenhouse gases concentration in the atmosphere, accumulation of stable organic contaminants in water ecosystems and exhaustion of natural resources.[3] Considering this, development of effective approaches for solar energy conversion for environmentally friendly chemical processes becomes a clear necessity for sustainable development.

The fundamental principles of photocatalysis involve three consecutive steps: photoexcitation where semiconductor materials absorb photons with energy equal to or greater than their bandgap, generating electron-hole pairs; charge separation and migration of these photogenerated carriers to the catalyst surface; and surface redox reactions where electrons and holes participate in reduction and oxidation processes, respectively.[4,5] This mechanism enables photocatalysis to offer a complex solution for producing valuable synthetic fuels, neutralizing harmful emissions and cleaning the environment.[2,6]

However, the main limitation for practical implementation of photocatalytic processes is the lack of effective photocatalysts that could function efficiently under sunlight. This is primarily caused by three fundamental challenges: a weak visible light absorption, rapid recombination of photogenerated electron-hole pairs, and slow surface reaction kinetics.[7,8] Graphitic carbon nitride (g-C_3N_4) stands out among other modern photocatalysts due to its unique combination of properties: metal-free nature, great chemical stability, ability to absorb visible light and simple synthesis routes from accessible precursors.[2,9] However, the drawbacks of fast charge carriers' recombination, insufficient surface area and limited electron conductivity significantly reduce the effectiveness of this material.

MXenes are a class of 2D materials that includes carbides and nitrides of transition metals.[10] They can be viewed as excellent partners for g-C_3N_4 for construction of new generation composite photocatalysts.[11] Owing to their exceptional electronic conductivity, tunable surface properties with different terminal groups (-OH, -O, -F) and high surface area, MXenes can form effective heterostructures with g-C_3N_4, leading to a synergetic effect that radically improves photocatalytic activity.[12–14] The wide spectrum of applications for MXene/g-C_3N_4 composites, such as hydrogen production, CO_2 reduction and pollutant degradation show their universal effectiveness for different photocatalytic areas.[11]

The aim of this review is to systematically summarize recent achievements in the synthesis and application of MXene/g-C_3N_4-based photocatalytic systems for different processes. This work summarizes modern synthesis methods as well as electron transfer mechanisms, and also discusses the potential applications of these materials for environmental and energy purposes. This comprehensive approach allows to fairly demonstrate the potential of MXene/g-C_3N_4-based composites as new generation photocatalysts to make a contribution to the development of sustainable technologies. To fully understand these composites, it is essential first to examine the properties of the individual components, beginning with graphitic carbon nitride.

Graphitic carbon nitride

Graphitic carbon nitride is a metal-free polymeric semiconductor with a macroheterocycle structure (Figure 1) that leads to outstanding photocatalytic properties.[2,15] Structurally, g-C_3N_4 resembles graphene and has a two-dimensional delocalized conjugated structure that is primarily composed of tri-s-triazine fragments (C_6N_7) linked by tertiary amines to form layered planes that are stacked onto each other by the formation of weak Van-der-Waals interactions.[16] In-plane structure contains various functional fragments, such as NH_2 and NH groups that can act as sites for CO_2 activation and conversion.[17] The unique structure of g-C_3N_4 leads to the average band gap of ~2.7 eV, which is suitable for visible light absorption and effective sunlight usage.[18] The positions of conduction and valence bands also lead to high enough red-ox potentials of photoinduced electron-hole pairs, so this material can be used for the whole variety of photocatalytic applications, as mentioned earlier.[19,20] Moreover, stable intraplane covalent bonds lead to high chemical and thermal stability of g-C_3N_4 sheets (up to 600°C in air).[21]

Traditionally, g-C_3N_4 is synthesized by thermal polycondensation of nitrogen-rich precursors, such as urea, dicyandiamide and melamine.[22] This process is usually conducted in temperatures around 500-600 °C in air or in inert atmosphere.[23] It is established that under high temperatures polymerization occurs with the formation of different intermediates.[24] However, these intermediates cannot be fully removed from the forming g-C_3N_4 due to incomplete polymerization, which in turn leads to a disorder in crystal structure. Consequentially, this leads to fast recombination of photogenerated charge carriers and limits photocatalytic activity. To solve this problem, more complicated synthesis routes may be utilized.

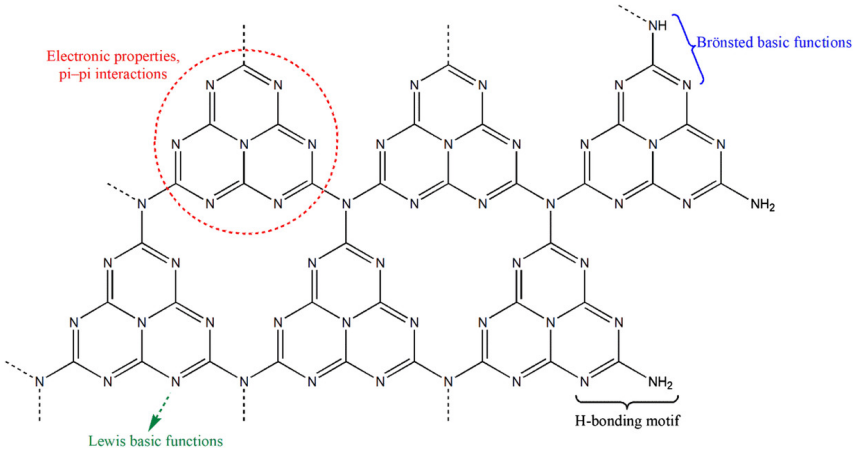

Figure 1. In-plane structure of g-C_3N_4 with various functional fragments.[15]

An additional way to boost photocatalytic properties of g-C_3N_4 is exfoliation. Similar to graphite, g-C_3N_4 can be exfoliated to single two-dimensional nanosheets by different means like thermal oxidation or acoustic energy of ultrasonic waves to overcome Van-der-Waals forces but to keep the C-N bonds intact.[28,29] Obtained nanosheets could be stored in acids or alkali to keep them from forming bonds with each other again. Interestingly, g-C_3N_4 nanosheets have a better in-plane electron mobility and bigger band gap than the bulk g-C_3N_4 due to the quantum size effect.[30] Consequentially, photogenerated charge carriers are less likely to recombine and have higher lifetime. The obvious drawback of this method is instability of exfoliated nanosheets that are very likely to come back to the multilayered structure if not kept in proper conditions.

A significant problem of the bulk g-C_3N_4 is poor charge separation and transfer.[31] Naturally, weak Van-der-Waals interactions between the layers impede the interplanar charge transfer.[32] But on top of it, incomplete polymerization leads to some heptazine rings being connected by hydrogen bonds, with the terminal amino groups acting as charge centers, thereby also hindering intraplanar charge transmission.[33] To circumvent this issue creating heterojunctions with other semiconductors or with conductors to add alternative electron transfer routes is an effective way to boost charge separation and increase the quantum efficiency.

Synthetic approaches to creating MXene/g-C_3N_4 composites

Among a wide variety of different types of materials that can be used for creating composite photocatalysts, MXenes are a relatively new class of materials that was first reported in literature in 2011 by Naguib *et al.*[34] This class consists of metal carbides, nitrides and carbonitrides (Figure 2) that are generally produced by MAX-phase (*e.g.* Ti_3AlC_2) etching, usually with HF solution or with in situ HF (LiF+HCl).[2] Important to note that different synthesis methods lead to different surface terminations (*e.g.* -O, -F, -OH, -Cl) which can heavily influence the properties of MXenes, including band gap size.[35–37] Generally, MXenes' high conductivity, hydrophilicity, ordered layered structure and tunable functional groups make them a very attractive material for photocatalyst design.[38,39] Moreover, MXenes usually have a high work function that makes them suitable for creating heterojunctions with g-C_3N_4.[40]

Quality and photocatalytic properties of g-C_3N_4/MXene composites are critically dependent on synthesis methods. The main goal when creating such heterostructure lies in ensuring the closest possible interaction for effective electron transfer. Presently used synthesis approaches can mostly be divided in three main types.

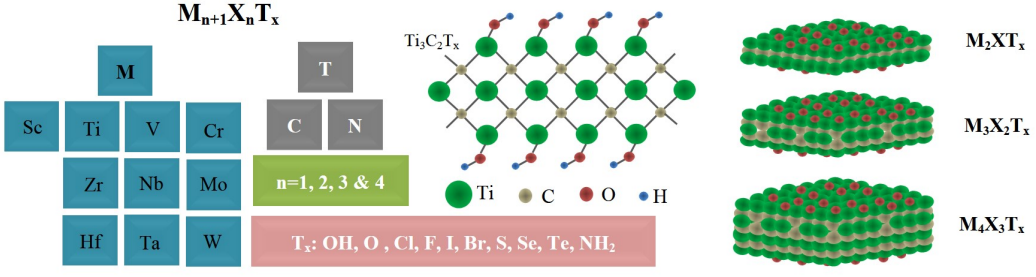

Figure 2. MXenes' general formula and structure.[11]

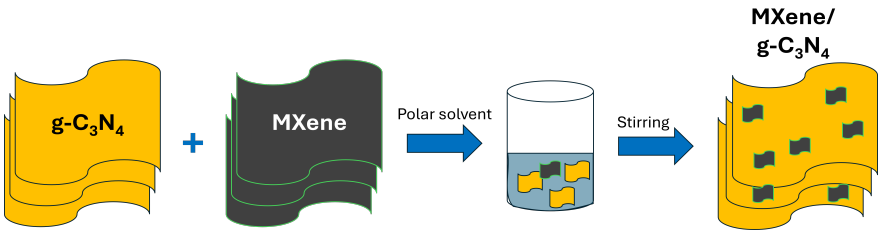

Figure 3. Schematic synthesis route of physical mixing method.

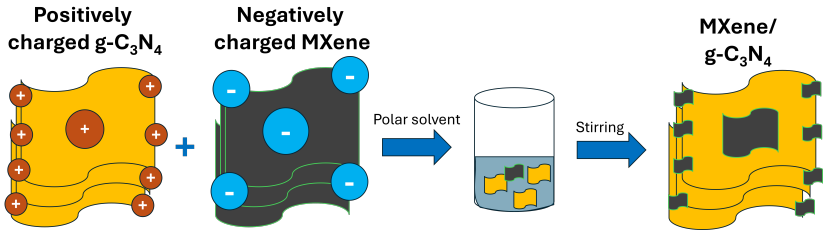

Figure 4. Schematic synthesis route of electrostatic self-assembly.

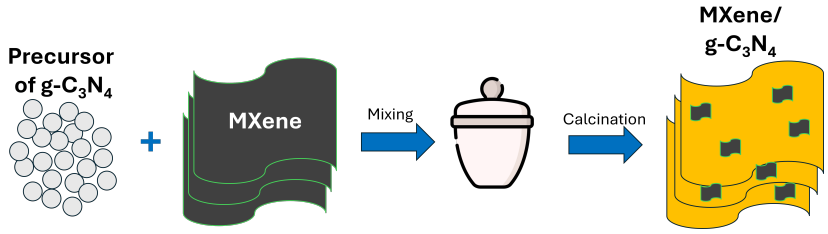

Figure 5. Schematic synthesis route of in situ thermal polymerizaiton.

Physical mixing

The most straightforward approach is to mix two pre-prepared components in a liquid medium with subsequent evaporation of a solvent (Figure 3). Multi-layered MXene is dispersed together with g-C_3N_4 in a polar solvent (water, ethanol, isopropanol), usually with ultrasound treatment, and a uniform suspension is obtained.[41–43] Then this suspension is either simply stirred or ultrasound is applied for longer periods of time. Since MXenes are not stable, solvent should be evaporated in a vacuum oven at 60–80 °C or via freeze drying. The main advantages of this method are its simplicity, reproducibility, precise control over component ratios and minimal influence on original structure of the components. However, the contact between components is relatively weak since chemical bonds are unlikely to be formed.

Electrostatic self-assembly

This is one of the most popular methods that is based on physically mixing the pre-synthesized components modified with charged surface groups in a solution.[42–55] Basically, multi-layered MXene with negatively charged surface groups (-O, -OH, -F) is dispersed in a polar solvent by ultrasound treatment to obtain a stable colloid suspension (Figure 4). Separately the surface of g-C_3N_4 is functionalized with positively charged groups (*e.g.* via protonating with HCl). When slowly mixing these two suspensions in an environment with a controlled pH, electrostatic attraction between oppositely charged surfaces leads to a spontaneous self-assembly of components. Afterwards, the resulting suspension should be washed to remove side ions and dried in a careful manner as described earlier. This method allows for tight contact between components and ordered structure with controlled morphology. On the other hand, synthesis conditions should be tightly controlled since otherwise an undesirable aggregation of components may occur.

Thermal polymerization in situ

This approach implies synthesis of g-C_3N_4 in presence of prepared MXene (Figure 5). Basically, MXene is mixed with a g-C_3N_4 precursor (*e.g.* melamine or urea) and is subjected to calcination at usual temperatures of 500–550 °C. However, high temperatures may lead to partial oxidation of MXenes, so using inert atmosphere, such as nitrogen or argon, is highly preferable.[58–63] During polymerization, layers of g-C_3N_4 form on top of MXene's surface resulting in a close contact with a possibility of chemical bonding. Although, this method makes it harder to control the degree of polymerization and limits the precursors that can be used for synthesis. Moreover, MXene degradation can still happen even in inert atmosphere, influencing the electronic structure of the resulting compo-

site. However, this influence can sometimes be beneficial. For example, multiple papers have shown that calcination of Ti_3C_2 leads to formation of *in situ* TiO_2/Ti_3C_2 junction that greatly increases photocatalytic activity.[64–67]

Main photocatalytic applications of MXene/g-C_3N_4 composites

Composites based on MXenes and g-C_3N_4 can open up new possibilities for different photocatalytic applications demonstrating promising effectiveness for various reactions.[11] Thanks to synergetic interaction of these components: semiconductor properties of g-C_3N_4 for generating electron-hole pairs under visible light combined with metallic and surface properties of MXenes acting as an effective electron acceptor or mediator.[68,69] This interaction not only hinders the recombination of photogenerated charge carriers but also creates new active centres for catalytic transformations. This chapter covers three photocatalytic applications that are reported the most in literature: H_2 generation, pollutant degradation and CO_2 reduction.

Hydrogen production

Molecular hydrogen possesses the highest known energy density among chemical fuels (120 MJ/kg) and thanks to its environmentally clean burning process it can be viewed as one of the key elements for sustainable energetics.[70] Today, however, H_2 is usually obtained through steam-methane reforming, which is a process followed by significant CO_2 emissions.[71,72] This is why photocatalytic water splitting under sunlight would be a perfect alternative that would allow to directly transform solar energy into chemical energy. Theoretically, energy of 1.23 eV is enough to split water into H_2 and O_2 (Equations 1–2, potentials at p*H*=7) but on practice a certain overpotential is required to drive the photoinduced electrons and holes through the interface and promote the red-ox reactions.[70]

$$2H_2O \rightarrow O_2 + 4H^+ + 4e^- \qquad E^0 = 1.23\ V_{NHE} \qquad (1)$$

$$2H^+ + 2e^- \rightarrow H_2 \qquad E^0 = 0\ V_{NHE} \qquad (2)$$

Traditionally, metal cocatalysts like Pt have been used to boost H_2 and O_2 generation efficiency.[73] However, MXene-based composites aside from aforementioned advantages can also exhibit hydrophilic properties, which would substantially boost wettability and mass transfer of reagents to active centres.[74] Comparison of binary MXene/g-C_3N_4 photocatalysts with different synthesis methods, reaction conditions and photocatalytic activity in H_2 production reaction reported in recent years is presented in Table 1.

Potapenko *et al.* synthesized $Ti_3C_2T_x$/g-C_3N_4 by a simple method of mixing pre-prepared g-C_3N_4 with Ti_3C_2 "ink" suspension obtained during Ti_3C_2 synthesis.[75] The effect of different organic electron donors (TEOA, ethanol, glucose) on activity under visible light irradiation was investigated. For all donors the addition of MXenes led to a significant increase in H_2 generation activity up to 98.4 $\mu mol \cdot g^{-1}h^{-1}$ for TEOA solution, which is a 37.8-times boost compared to pristine g-C_3N_4. This increase was explained by formation of a Schottky barrier between the two components, with Ti_3C_2 effectively acting as a metal co-catalyst. Ti_3C_2 has a higher work function than g-C_3N_4, so the contact would lead to electron diffusion in the direction of Ti_3C_2 and the energy bands would bend upwards at the interface (Figure 6).[80,87] Thus, photogenerated electrons would accumulate on the surface of MXenes and participate in the H^+ reduction while as holes would remain on g-C_3N_4 and partake in oxidation reactions with electron donors. This way effective charge separation is achieved and charge recombination rate is reduced.[88]

Xu *et al.* employed protonation of g-C_3N_4 by dispersing it in HCl and then mixed it with Ti_3C_2 MXenes with ultrasonic treatment.[43] This approach allowed to alter both surface morphology of g-C_3N_4 and its band structure leading to H_2 production rate of 727 $\mu mol \cdot g^{-1}h^{-1}$. Another effective way of modifying g-C_3N_4 structure is non-metallic doping. Introducing impurities is a common way to reduce band gap in semiconductors and improve conductivity.[89] In particular, doping with P, B and S elements has been shown to be effective in increasing activity of g-C_3N_4/Ti_3C_2 photocatalysts.[80,82,83]

Especially high activity can be achieved if another co-catalyst is introduced into the system. A number of works describes a method of in-situ Pt photo-deposition by adding H_2PtCl_6 to a solution of electron donor.[79,82,83,85,86] When light is turned on, Pt particles are reduced on the surface of the photocatalyst and start influencing the electron transfer schemes. Xu *et al.* prepared Ti_3CN MXenes and defective g-C_3N_4 to synthesize Ti_3CN/g-C_3N_4 composites via electrostatic self-assembly. With in-situ deposited Pt the rate of photocatalytic H_2 generation reached 7630.5 $\mu mol \cdot g^{-1}h^{-1}$, and authors highlighted high conductivity of Ti_3CN and strong interfacial coupling of the two components.

Pollutant degradation

Another serious environmental threat in modern world is water pollution by persistent organic pollutants, such as synthetic dyes, pharmaceuticals and antibiotics.[90] Traditional water purification methods are often not effective enough to cause complete degradation of these stable compounds, so they tend to accumulate in the environment and become a part of food chains leading to detrimental effect for human health.[91,92] Photocatalytic oxidation under the sunlight can be viewed as a perspective cost-effective and ecologically sustainable alternative.[90,93,94] The mechanism for this process involves oxidation of a contaminant by reactive oxygen species that are produced with photogenerated electrons and holes in accordance to Equations 3–4.

$$H_2O + h^+ \rightarrow OH^{\bullet} + H^+ \qquad (3)$$

$$O_2 + e^- \rightarrow O_2^- \qquad (4)$$

Thus, both holes and electrons can directly influence the activity in a target degradation reaction, making charge separation very important. Comparison of binary MXene/g-C_3N_4 photocatalysts with different synthesis methods, reaction conditions and removal efficiencies for various types of organic pollutants reported in recent years is presented in Table 2.

Table 1. Comparison of MXene/g-C_3N_4 photocatalytic systems for H_2 generation reported in recent years.

Photocatalyst	Composite synthesis method	Light source	Reaction medium	H_2 formation rate, $\mu mol \cdot g^{-1}h^{-1}$	Ref.
Ti_3C_2/g-C_3N_4	Physical mixing	430 nm LED	30 vol% TEOA 10 vol% C_2H_5OH 0.2M $C_6H_{12}O_6$	98.4 24.0 7.9	[75]
3D/2D Ti_3C_2/g-C_3N_4	Polymerization in situ	300W Xe lamp, 420 nm filter	10 vol% TEOA	116	[76]
2D/2D Ti_3C_2/g-C_3N_4	Electrostatic self-assembly	200W Hg lamp, 400 nm filter	10 vol% TEOA	72.3	[77]
$Ti_3C_2T_x$ with oxidized surface groups/g-C_3N_4	Mechanical mixing	350W Xe lamp, 400 nm filter	10 vol% TEOA	88	[78]
Plasma-treated $Ti_3C_2T_x$/g-C_3N_4	Mechanical mixing	350W Xe lamp, 400 nm filter	10 vol% TEOA	17.8	[42]
Ti_3C_2/protonated g-C_3N_4	Ultrasound-assisted mixing	300W Xe lamp, 420 nm filter	10 vol% TEOA	727	[43]
2D/2D Ti_3CN/g-C_3N_4	Electrostatic self-assembly	300W Xe lamp	10 vol% TEOA + H_2PtCl_6	7630	[79]
2D/1D Ti_3C_2/P-doped g-C_3N_4	Electrostatic self-assembly	300W Xe lamp	20 vol% CH_3OH	565	[80]
2D/2D V_2C/g-C_3N_4	Physical mixing	35W Xe HID lamp, 420 nm filter, 20 mW cm^{-2}	5 vol% CH_3OH	360	[81]
2D/2D Ti_3C_2/S-doped g-C_3N_4	Ultrasound-assisted mixing	300W Xe lamp, 420 nm filter, 100 mW cm^{-2}	10 vol% TEOA + H_2PtCl_6	3180	[82]
2D/2D Ti_3C_2/B-doped g-C_3N_4	Electrostatic self-assembly	300W Xe lamp, 400 nm filter	10 vol% CH_3OH + H_2PtCl_6	1990	[83]
$Ti_3C_2Cl_2$/g-C_3N_4	Electrostatic self-assembly	300W Xe lamp, 420 nm filter	10 vol% TEOA	156	[84]
2D/3D Ti_3C_2/g-C_3N_4	Electrostatic self-assembly	300W Xe lamp, 420 nm filter	10 vol% TEOA + H_2PtCl_6	1950	[85]
$Ti_3C_2T_x$/crystalline g-C_3N_4	Ultrasound-assisted mixing	300W Xe lamp, 420 nm filter	10 vol% TEOA + H_2PtCl_6	2650	[86]

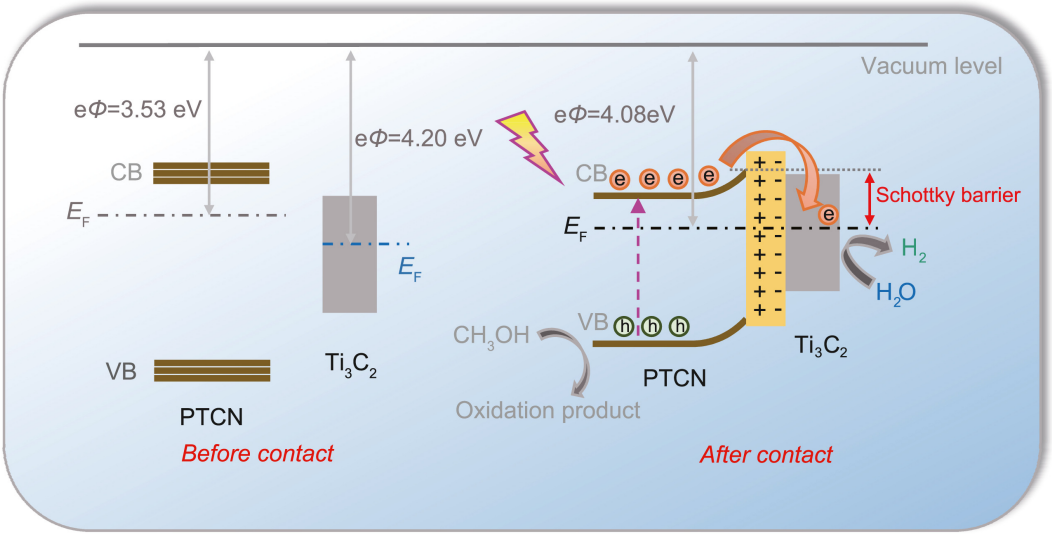

Figure 6. Proposed electron transfer mechanism for g-C_3N_4/Ti_3C_2 junction in photocatalytic H_2 production. PTCN – P-doped tubular g-C_3N_4.[80]

Ya *et al.* developed an effective approach for degradation of Rhodamine B by regulating the vapor pressure in the autoclave via discontinuing the hydrothermal process to achieve high porosity of g-C_3N_4.[103] Obtained g-C_3N_4 microtubes with an extremely high surface area of 153 m^2/g were coupled with $Ti_3C_2T_x$ via electrostatic self-assembly and tested under visible light. Thanks to the morphology of g-C_3N_4 and the formation of efficient heterojunction, 98% removal of Rhodamine B under visible light irradiation could be achieved in 1 hour. Another effective approach was employed by Liu *et al.,* who synthesized 3D interconnected porous g-C_3N_4 via one-step thermal polymerization of melamine and cyanuric acid, and combined it with Ti_3C_2 MXenes via electrostatic self-assembly.[85] Using a 500W halide lamp with a visible light filter, complete removal of Rhodamine B is reported to be achieved in only 25 minutes of irradiation time. Supposed scheme of photocatalytic pollutant degradation is shown in Figure 7.[106]

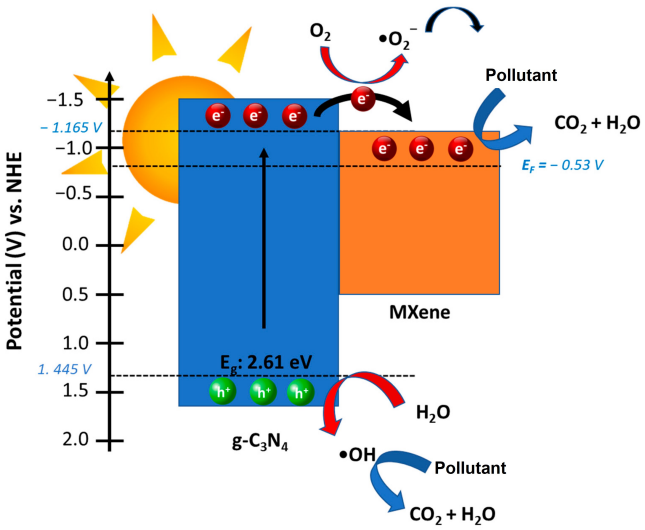

Figure 7. Proposed electron transfer route for Ti_3C_2/g-C_3N_4 during photocatalytic pollutant degradation.[106]

Table 2. Comparison of MXene/g-C_3N_4 photocatalytic systems for pollutant degradation reported in recent years.

Photocatalyst	Composite synthesis method	Light source	Irradiation time	Photocatalyst concentration	Pollutant, initial concentration	Removal, %	Ref.
2D/3D Ti_3C_2/g-C_3N_4	Electrostatic self-assembly	500 W halide lamp, 420 nm filter, 30 mW· cm^{-2}	25 min	0.5 g·L^{-1}	Rhodamine B, 20 mg·L^{-1}	100	[85]
2D/2D Ti_3C_2/S-doped g-C_3N_4	Ultrasound-assisted mixing	300 W Xe lamp, 420 nm filter, 100 mW·cm^{-2}	1 h	0.1 g·L^{-1}	Levofloxacin, 10 mg·L^{-1}	100	[82]
Ti_3C_2/g-C_3N_4	Physical mixing	500 W halogen lamp	3 h	5 g·L^{-1}	Methylene blue, 10 mg·L^{-1}	69.4	[95]
2D Ti_3C_2/g-C_3N_4	Electrostatic self-assembly	300 W Xe lamp, 420 nm filter	1 h	Not specified	Tetracycline, 20 mg·L^{-1}	93.9	[96]
Ti_3C_2/g-C_3N_4	Ultrasound-assisted mixing	300 W Xe lamp, 400 nm filter	3.5 h	2 g·L^{-1}	Ciprofloxacin, 10 mg·L^{-1}	97.8	[97]
Ti_3C_2/supramolecular g-C_3N_4	Ultrasound-assisted mixing	300 W Xe lamp, 420 nm filter	2.5 h	0.1 g·L^{-1}	Arbidol hydrochloride, 10 g·L^{-1}	99	[98]
Magnetic $Ti_3C_2T_x$/g-C_3N_4	Physical mixing	150W high-pressure lamp, 100 mW·cm^{-2}	2 h	10 mg·L^{-1}	Clindamycin, 125 mg·L^{-1}	92	[99]
V_2C/g-C_3N_4	Ultrasound-assisted mixing	300 W Xe lamp	2 h	1 g·L^{-1}	Methyl orange, 10 mg·L^{-1}	94.5	[100]
Ti_3C_2-SO_3H/g-C_3N_4	Ultrasound-assisted mixing	35 W Xe lamp	2 h	0.6 g·L^{-1}	Tetracycline hydrochloride, 10 mg·L^{-1}	75.4	[101]
g-C_3N_4/Ti_3C_2	Physical mixing	500 W halogen lamp	2.5 h	2 g·L^{-1}	Methylene blue, 30 ppm	100	[102]
2D/1D $Ti_3C_2T_x$/g-C_3N_4	Electrostatic self-assembly	300 W Xe lamp, 420 nm filter, 100 mW·cm^{-2}	1 h	0.2 g·L^{-1}	Rhodamine B, 20 mg·L^{-1}	98	[103]
Ti_3C_2/g-C_3N_4	Ultrasound-assisted mixing	300W Xe lamp, 420 nm filter	30 min	0.4 g·L^{-1}	Levofloxacin, 20 mg·L^{-1}	72	[104]
Ti_3C_2/g-C_3N_4	Polymerization in situ	300W Xe lamp, 420 nm filter	40 min	0.2 g·L^{-1}	Tetracycline, 15 mg·L^{-1}	90.1	[105]

Table 3. Comparison of MXene/g-C_3N_4 photocatalytic systems for CO_2 reduction reported in recent years.

Photocatalyst	Composite synthesis method	Light source	Conditions	Product formation rate, μmol·g^{-1}h^{-1}	Ref.
Ti_3C_2/g-C_3N_4	Ultrasound-assisted mixing	300W Xe lamp, 420 nm filter	Gas phase, CO_2+H_2O	CO, 10.7 CH_4, 4.19	[104]
$Ti_3C_2T_x$/mesoporous g-C_3N_4	Co-annealing	300W Xe lamp	Gas phase, CO_2 + H_2O	CH_4, 2.11	[110]
2D/1D $Ti_3C_2T_x$/g-C_3N_4	Ultrasound-assisted mixing	300W Xe lamp	Gas phase, CO_2 + H_2O	CO, 0.73 CH_4, 1.4	[111]
2D Ti_3C_2/porous g-C_3N_4	Electrostatic self-assembly	300W Xe lamp, 420 nm filter	Gas phase, CO_2 (0.6 MPa) + H_2O, 60°C	CH_4, 0.99	[112]
2D/2D V_2C/g-C_3N_4	Physical mixing	35W HID Xe lamp, 20 mW cm^{-2}	Gas phase, flow reactor, CO_2 + H_2O	CO, 37.8 CH_4 51.3	[113]
$Ti_3C_2(OH)_2$/g-C_3N_4	Physical mixing	300W Xe lamp, 420 nm filter	Gas phase, CO_2 + H_2O	CO, 11.2 CH_4, 0.20	[114]
2D/2D Ti_3C_2/g-C_3N_4	Polymerization in situ	300W Xe lamp, 420 nm filter	Gas phase, Na-HCO_3 + H_2SO_4	CO, 5.19 CH_4, 0.04	[115]

Xu *et al.* used a simple sonication-assisted mixing to modify g-C_3N_4 with V_2C MXene for degradation of methyl orange.[100] Despite receiving a lot less attention than Ti_3C_2, V_2C has a similar morphology but a higher specific surface area with more active centres.[107] V_2C also has a suitable electronic structure to accept photogenerated electrons from g-C_3N_4 in a similar manner to Ti_3C_2. Utilizing the synergistic effect of this heterojunction, 94.5% removal of methyl orange in 2 hours could be achieved. Saafie *et al.* prepared g-C_3N_4/Ti_3C_2 by wet impregnation for degradation of methylene blue.[102] Usually, Ti_3C_2 is reported to exhibit metallic properties and is used as a modifying component with weight ratios less than 10%, however in this paper MXene had a calculated band gap of 1.23 eV and was used as a main component, with 0.4 wt% of g-C_3N_4. In this scheme Ti_3C_2 can be viewed as a semiconductor with a narrow band gap and would also be generating excited electrons under irradiation. With such heterostructure photocatalyst complete removal of methylene blue was achieved after 2.5 hours of reaction.

CO_2 reduction

In the context of constantly increasing CO_2 emissions development of environmentally safe and energy-effective means of CO_2 conversion to valuable chemical products is one of the most relevant modern problems.[2] Photocatalytic CO_2 reduction imitates natural photosynthesis and allows not only to decrease the CO_2 concentration in the atmosphere but also obtain a variety of different organic compounds, such as formic acid, CO, formaldehyde, methanol, methane or even ethane (Equations 5-10, potentials at p*H*=7), that could be used for synthetic purposes and in chemical industry.[108,109]

$$CO_2 + 2H^+ + 2e^- \rightarrow HCOOH \qquad E^0 = -0.66\ V_{NHE} \quad (5)$$

$$CO_2 + 2H^+ + 2e^- \rightarrow CO + H_2O \qquad E^0 = -0.52\ V_{NHE} \quad (6)$$

$$CO_2 + 4H^+ + 4e^- \rightarrow CH_2O + H_2O \qquad E^0 = -0.49\ V_{NHE} \quad (7)$$

$$CO_2 + 6H^+ + 6e^- \rightarrow CH_3OH + H_2O \qquad E^0 = -0.40\ V_{NHE} \quad (8)$$

$$CO_2 + 8H^+ + 8e^- \rightarrow CH_4 + 2H_2O \qquad E^0 = -0.25\ V_{NHE} \quad (9)$$

$$2CO_2 + 14H^+ + 14e^- \rightarrow C_2H_6 + 4H_2O \qquad E^0 = -0.27\ V_{NHE} \quad (10)$$

However, as can be seen in Table 3, for binary MXene/g-C_3N_4 photocatalysts only two products were reported: CO and CH_4. Still, when using these photocatalysts as a base for novel tertiary composites in future studies, selectivity along with activity could change dramatically.

Among all possible surface functional groups on MXenes, the hydroxyl ones are probably the most attractive for photocatalytic CO_2 reduction since they heavily improve effectiveness of adsorption of CO_2 molecules.[116] Hence, Tang *et al.* mixed the alkalized Ti_3C_2 with g-C_3N_4 in aqueous solution to obtain composite photocatalysts for CO_2 reduction.[41] The highest obtained CO production rate was 11.2 μmol·g^{-1}h^{-1} which is 5.9 times higher compared to unmodified g-C_3N_4. This increase in activity is explained by excellent electric conductivity of $Ti_3C_2(OH)_2$ and a huge difference in Fermi level positions of the components (-2.69 V for $Ti_3C_2(OH)_2$ and -0.223 V for g-C_3N_4), which leads to a reliable charge separation. Madi *et al.* prepared V_2C/g-C_3N_4 nanosheet photocatalyst for testing in CO_2 reduction reaction in a fixed-bed reactor and achieved production rates of 37.8 and 51.3 μmol·g^{-1}h^{-1} for CO and CH_4 respectively.[113] They also compared the activity of V_2AlC/g-C_3N_4 and it turned out to be only slightly lower (37.0 and 46.3 for CO and CH_4 respectively). This indicates that while etching of MAX-phases does lead to improvement of photocatalytic properties, they are not very significant. It is also worth noting that despite seemingly high activity most photocatalytic experiments are usually conducted in static reactors and when comparing the results with flow reactors caution should be exercised.

Conclusions

Conducted analysis of modern researches clearly indicates that composites based on MXenes and g-C_3N_4 are a highly perspective class of photocatalytic materials with potential for a wide variety of applications. Combination of special properties of these components, such as the ability of g-C_3N_4 to effectively absorb visible light to generate excited electron-hole pairs, together with high electric conductivity and surface area of MXenes, leads to a great synergetic effect boosting photocatalytic activity. Main advantages of MXene/g-C_3N_4 composites include effective separation of photoinduced charge carriers due to formation of a heterojunction (usually Schottky junction) leading to increased lifetime of electrons and holes and the possibility of controlling electric and surface properties of MXenes by varying synthesis approaches to better fit the needed process. In particular, the main discussed synthesis methods – physical mixing, electrostatic self-assembly and in situ polymerization – are all viable methods to obtain different morphologies of composites with all kinds of combinations of 1D, 2D and 3D materials.

Probably the most promising direction for future research is creation of ternary photocatalytic systems with the addition of other popular photocatalytic materials, such as metal oxides, metals or metal organic frameworks, to further increase the spectrum of absorbed light and to increase the effectiveness of catalytic active sites. It could either be a system MXene/g-C_3N_4/semiconductor or MXene/g-C_3N_4/metal nanoparticles, as both variants would open new possibilities for engineering complex electron transfer schemes and enhancing the synergetic effect. Other important goals for future research are still development of scalable synthesis methods, increase of photocatalyst stability in real application conditions and deeper investigation of reaction mechanisms and interaction of components on atomic scale. Use of modern methods of in situ characterization and computer modelling could allow to determine precise dependencies between structure and properties to clearly reveal a way to create new generations of highly effective photocatalysts to solve relevant energetical and environmental problems.

Acknowledgements. This work was supported by the Russian Science Foundation (grant no. 24-13-00416).

References

1. Li C., Cao Q., Wang F., Xiao Y., Li Y., Delaunay J.J., Zhu H. *Chem. Soc. Rev.* **2018**, *47*, 4981–5037, doi: 10.1039/C8CS00067K.
2. Alekseev R.F., Saraev A.A., Kurenkova A.Y., Kozlova E.A. *Russ. Chem. Rev.* **2024**, *93*, 5124, doi: 10.59761/RCR5124.
3. Kumar A., Rana S., Sharma G., Dhiman P., I. Shekh M., Stadler F.J. *J. Environ. Chem. Eng.* **2023**, *11*, 110770, doi: 10.1016/J.JECE.2023.110770.
4. Ishaq T., Yousaf M., Bhatti I.A., Batool A., Asghar M.A., Mohsin M., Ahmad M. *Int. J. Hydrogen Energy* **2021**, *46*, 39036–39057, doi: 10.1016/J.IJHYDENE.2021.09.165.
5. Raizada P., Soni V., Kumar A., Singh P., Parwaz Khan A.A., Asiri A.M., Thakur V.K., Nguyen V.H. *J. Mater.* **2021**, *7*, 388–418, doi: 10.1016/J.JMAT.2020.10.009.
6. Rana P., Soni V., Kumar R., Chawla A., Parwaz Khan A.A., Singh P., Thakur S., Raizada P., Alzahrani K.A. *Fuel* **2025**, *386*, 134286, doi: 10.1016/J.FUEL.2025.134286.
7. Ren H., Labidi A., Chang T., Miao Z., Feng X., Wang C. *Coord. Chem. Rev.* **2026**, *548*, 217183, doi: 10.1016/J.CCR.2025.217183.
8. Mehrpooya M., Bayatlar F. *Arch. Comput. Methods Eng.* **2025**, 1–53, doi: 10.1007/S11831-025-10381-X.
9. Tofil H.M., Ghazi R., Ghaib F.A., Dara R.N., Kebaili I., Boukhris I., Ding H., Rehman Z. *Sustain. Energy Fuels* **2025**, *9*, 2900–2927, doi: 10.1039/D4SE01620C.
10. Cai Y., Xiao F.X. *Acta Physico-Chimica Sin.* **2024**, *40*, 2306048, doi: 10.3866/PKU.WHXB202306048.
11. Akhoondi A., Mirzaei M., Nassar M.Y., Sabaghian Z., Hatami F., Yusuf M. *Synth. Sinter.* **2022**, *2*, 151–169, doi: 10.53063/SYNSINT.2022.24121.
12. Khan K., Tareen A.K., Iqbal M., Hussain I., Mahmood A., Khan U., Khan M.F., Zhang H., Xie Z. *J. Mater. Chem. A* **2023**, *11*, 19764–19811, doi: 10.1039/D3TA03069E.
13. Ali M.M., Hossen M.A., Aziz A.A. *J. Environ. Chem. Eng.* **2025**, *13*, 116877, doi: 10.1016/J.JECE.2025.116877.
14. Mozafari M., Soroush M. *Mater. Adv.* **2021**, *2*, 7277–7307, doi: 10.1039/D1MA00625H.
15. Fidan T., Torabfam M., Saleem Q., Wang C., Kurt H., Yüce M., Tang J., Bayazit M.K. *Adv. Energy Sustain. Res.* **2021**, *2*, 2000073, doi: 10.1002/AESR.202000073.
16. Kessler F.K., Zheng Y., Schwarz D., Merschjann C., Schnick W., Wang X., Bojdys M.J. *Nat. Rev. Mater.* **2017**, *2*, 17030, doi: 10.1038/natrevmats.2017.30.
17. Su Q., Sun J., Wang J., Yang Z., Cheng W., Zhang S. *Catal. Sci. Technol.* **2014**, *4*, 1556–1562, doi: 10.1039/C3CY00921A.
18. Zhou Z., Zhang Y., Shen Y., Liu S., Zhang Y. *Chem. Soc. Rev.* **2018**, *47*, 2298–2321, doi: 10.1039/C7CS00840F.
19. Zhang X., Jiang S.P. *Mater. Today Energy* **2022**, *23*, 100904, doi: 10.1016/J.MTENER.2021.100904.
20. Ong W.J., Tan L.L., Ng Y.H., Yong S.T., Chai S.P. *Chem. Rev.* **2016**, *116*, 7159–7329, doi: 10.1021/acs.chemrev.6b00075.
21. Darkwah W.K., Oswald K.A. *Nanoscale Res. Lett.* **2019**, *14*, 234, doi: 10.1186/S11671-019-3070-3.
22. Ye S., Wang R., Wu M.Z., Yuan Y.P. *Appl. Surf. Sci.* **2015**, *358*, 15–27, doi: 10.1016/J.APSUSC.2015.08.173.
23. Ramalingam M., Ponnusamy V.K., Sangilimuthu S.N. *Environ. Sci. Pollut. Res.* **2020**, *27*, 17481–17491, doi: 10.1007/S11356-019-05494-3.
24. Lin Z., Wang X. *Angew. Chemie Int. Ed.* **2013**, *52*, 1735–1738, doi: 10.1002/ANIE.201209017.
25. Xu R., Li J., Sui G., Zhuang Y., Guo D., Luo Z., Liang S., Yao H., Wang C., Chen S. *Appl. Surf. Sci.* **2022**, *578*, 152064, doi: 10.1016/J.APSUSC.2021.152064.
26. Mathias J.P., Simanek E.E., Zerkowski J.A., Seto C.T., Whitesides G.M. *J. Am. Chem. Soc.* **1994**, *116*, 4316–4325, doi: 10.1021/ja00089a021.
27. Jun Y.S., Lee E.Z., Wang X., Hong W.H., Stucky G.D., Thomas A. *Adv. Funct. Mater.* **2013**, *23*, 3661–3667, doi: 10.1002/ADFM.201203732.
28. Chen H.Y., Ruan L.W., Jiang X., Qiu L.G. *Analyst* **2015**, *140*, 637–643, doi: 10.1039/c4an01693a.
29. Niu P., Zhang L., Liu G., Cheng H.M. *Adv. Funct. Mater.* **2012**, *22*, 4763–4770, doi: 10.1002/ADFM.201200922.
30. Dong F., Li Y., Wang Z., Ho W.K. *Appl. Surf. Sci.* **2015**, *358*, 393–403, doi: 10.1016/J.APSUSC.2015.04.034.
31. Song T., Zhang X., Matras-Postolek K., Yang P. *Carbon N. Y.* **2023**, *202*, 378–388, doi: 10.1016/j.carbon.2022.11.008.
32. Xing W., Li C., Chen G., Han Z., Zhou Y., Hu Y., Meng Q. *Appl. Catal. B Environ.* **2017**, *203*, 65–71, doi: 10.1016/J.APCATB.2016.09.075.
33. Liu D., Chen S., Zhang Y., Li R., Peng T. *Appl. Catal. B Environ. Energy* **2023**, *333*, 122805, doi: 10.1016/j.apcatb.2023.122805.

34. Naguib M., Kurtoglu M., Presser V., Lu J., Niu J., Heon M., Hultman L., Gogotsi Y., Barsoum M.W. *Adv. Mater.* **2011**, *23*, 4248–4253, doi: 10.1002/ADMA.201102306.
35. Cheng L., Li X., Zhang H., Xiang Q. *J. Phys. Chem. Lett.* **2019**, *10*, 3488–3494, doi:10.1021/acs.jpclett.9b00736.
36. Anasori B., Lukatskaya M.R., Gogotsi Y. *Nat. Rev. Mater.* **2017**, *2*, 16098, doi: 10.1038/natrevmats.2016.98.
37. Naguib M., Mochalin V.N., Barsoum M.W., Gogotsi Y. *Adv. Mater.* **2014**, *26*, 992–1005, doi: 10.1002/adma.201304138.
38. Han X., An L., Hu Y., Li Y., Hou C., Wang H., Zhang Q. *Appl. Catal. B Environ.* **2020**, *265*, 118539, doi: 10.1016 /j.apcatb.2019.118539.
39. Gonzalez-Julian J. *J. Am. Ceram. Soc.* **2021**, *104*, 659–690, doi:10.1111/JACE.17544.
40. Koh S.W., Rekhi L., Arramel N., Birowosuto M.D., Trinh Q.T., Ge J., Yu W., Wee A.T.S., Choksi T.S., Li H. *ACS Appl. Mater. Interfaces* **2024**, *16*, 66826–66836, doi: 10.1021/acsami.3c11857.
41. Tang Q., Sun Z., Deng S., Wang H., Wu Z. *J. Colloid Interface Sci.* **2020**, *564*, 406–417, doi: 10.1016/J.JCIS. 2019.12.091.
42. Xu F., Zhang D., Liao Y., Wang G., Shi X., Zhang H., Xiang Q. *J. Am. Ceram. Soc.* **2020**, *103*, 849–858, doi: 10.1111/ JACE.16798.
43. Xu H., Xiao R., Huang J., Jiang Y., Zhao C., Yang X. *Chinese J. Catal.* **2021**, *42*, 107–114, doi: 10.1016/S1872-2067(20)63559-8.
44. Wen J., Xie J., Chen X., Li X. *Appl. Surf. Sci.* **2017**, *391*, 72–123, doi: 10.1016/J.APSUSC.2016.07.030.
45. Hu J., Ding J., Zhong Q. *J. Colloid Interface Sci.* **2021**, *582*, 647–657, doi: 10.1016/J.JCIS.2020.08.047.
46. Su T., Hood Z.D., Naguib M., Bai L., Luo S., Rouleau C.M., Ivanov I.N., Ji H., Qin Z., Wu Z. *Nanoscale* **2019**, *11*, 8138–8149, doi: 10.1039/C9NR00168A.
47. Wang X.X., Meng S., Zhang S., Zheng X., Chen S. *Catal. Commun.* **2020**, *147*, 106152, doi: 10.1016/j.catcom.2020. 106152.
48. Li Y., Ding L., Guo Y., Liang Z., Cui H., Tian J. *ACS Appl. Mater. Interfaces* **2019**, *11*, 41440–41447, doi: 10.1021/ acsami.9b14985.
49. Kamat P. V., Jin S. *ACS Energy Lett.* **2018**, *3*, 622–623, doi: 10.1021/acsenergylett.8b00196.
50. Song Q., Hu J., Zhou Y., Ye Q., Shi X., Li D., Jiang D. *J. Colloid Interface Sci.* **2022**, *623*, 487–499, doi: 10.1016/ J.JCIS.2022.05.064.
51. Yang Y., Zeng Z., Zeng G., Huang D., Xiao R., Zhang C., Zhou C., Xiong W., Wang W., Cheng M., Xue W., Guo H., Tang X., He D. *Appl. Catal. B Environ.* **2019**, *258*, 117956, doi: 10.1016/J.APCATB.2019.117956.
52. Kang J., Byun S., Kim S., Lee J., Jung M., Hwang H., Kim T.W., Song S.H., Lee D. *ACS Appl. Energy Mater.* **2020**, *3*, 9226–9233, doi: 10.1021/acsaem.0c01590.
53. Liu N., Lu N., Su Y., Wang P., Quan X. *Sep. Purif. Technol.* **2019**, *211*, 782–789, doi: 10.1016/J.SEPPUR.2018.10.027.
54. Chang B., Guo Y., Liu H., Li L., Yang B. *J. Mater. Chem. A* **2022**, *10*, 3134–3145, doi: 10.1039/D1TA09941H.
55. He J., Yang J., Jiang F., Liu P., Zhu M. *Chemosphere* **2020**, *258*, 127339, doi: 10.1016/j.chemosphere.2020.127339.
56. Zhou Y., Zhang C., Huang D., Wang W., Zhai Y., Liang Q., Yang Y., Tian S., Luo H., Qin D. *Appl. Catal. B Environ.* **2022**, *301*, 120749, doi: 10.1016/J.APCATB.2021.120749.
57. Lin S., Zhang N., Wang F., Lei J., Zhou L., Liu Y., Zhang J. *ACS Sustain. Chem. Eng.* **2021**, *9*, 481–488, doi: 10.1021/acssuschemeng.0c07753.
58. Li J., Li J., Wu C., Li Z., Cai L., Tang H., Zhou Z., Wang G., Wang J., Zhao L., Wang S. *Carbon N. Y.* **2021**, *179*, 387–399, doi: 10.1016/J.CARBON.2021.04.046.
59. Ran J., Gao G., Li F.T., Ma T.Y., Du A., Qiao S.Z. *Nat. Commun.* **2017**, *8*, 13907, doi: 10.1038/ncomms13907.
60. Li J., Zhang Q., Zou Y., Cao Y., Cui W., Dong F., Zhou Y. *J. Colloid Interface Sci.* **2020**, *575*, 443–451, doi: 10.1016/J.JCIS.2020.04.119.
61. Li S., Wang Y., Wang J., Liang J., Li Y., Li P. *J. Mol. Liq.* **2022**, *346*, 117937, doi: 10.1016/J.MOLLIQ.2021.117937.
62. Dong H., Zhang X., Zuo Y., Song N., Xin X., Zheng B., Sun J., Chen G., Li C. *Appl. Catal. A Gen.* **2020**, *590*, 117367, doi: 10.1016/J.APCATA.2019.117367.
63. Xie Y., Naguib M., Mochalin V.N., Barsoum M.W., Gogotsi Y., Yu X., Nam K.W., Yang X.Q., Kolesnikov A.I., Kent P.R.C. *J. Am. Chem. Soc.* **2014**, *136*, 6385–6394, doi: 10.1021/ja501520b
64. Low J., Zhang L., Tong T., Shen B., Yu J. *J. Catal.* **2018**, *361*, 255–266, doi: 10.1016/J.JCAT.2018.03.009.
65. Li Y., Yang Y.L., Chen G., Fan J.J., Xiang Q.J. *Rare Met.* **2022**, *41*, 3045–3059, doi: 10.1007/S12598-022-02007-Z/METRICS.
66. Li H., Song Q., Wan S., Tung C.W., Liu C., Pan Y., Luo G.Q., Chen H.M., Cao S., Yu J., Zhang L.M. *Small* **2023**, *19*, 2301711, doi: 10.1002/SMLL.202301711.
67. Song Q., Shen B., Yu J., Cao S. *ChemNanoMat* **2021**, *7*, 910–915, doi: 10.1002/CNMA.202100155.
68. Mandari K.K., Kang M. *Adv. Ind. Eng. Chem.* **2025**, *1*, 14, doi: 10.1007/S44405-025-00014-Z.
69. Subha N., Nagappagari L.R., Ravi Sankar A. *Nanotechnology* **2024**, *35*, 502002, doi: 10.1088/1361-6528/AD7E2F.
70. Kamat P. V., Bisquert J. *J. Phys. Chem. C* **2013**, *117*, 14873–14875, doi: 10.1021/JP406523W.
71. Taipabu M.I., Viswanathan K., Wu W., Hattu N., Atabani A.E. *Process Saf. Environ. Prot.* **2022**, *164*, 384–407, doi: 10.1016/J.PSEP.2022.06.006.
72. Iulianelli A., Liguori S., Wilcox J., Basile A. *Catal. Rev.* **2016**, *58*, 1–35, doi: 10.1080/01614940.2015.1099882.
73. Kamat P. V. *J. Phys. Chem. Lett.* **2012**, *3*, 663–672, doi: 10.1021/JZ201629P.
74. Yu L.P., Lu L., Zhou X.H., Xu L. *Adv. Mater. Interfaces* **2023**, *10*, 2201818, doi: 10.1002/ADMI.202201818.
75. Potapenko K.O., Vasilchenko D.B., Kurenkova A.Y., Saraev A.A., Mishchenko D.D., Gerasimov E.Y., Kozlova E.A. *Int. J. Hydrogen Energy* **2025**, *99*, 291–300, doi: 10.1016/ J.IJHYDENE.2024.12.213.
76. Li J., Zhao L., Wang S., Li J., Wang G., Wang J. *Appl. Surf. Sci.* **2020**, *515*, 145922, doi: 10.1016/J.APSUSC.2020.145922.
77. Su T., Hood Z.D., Naguib M., Bai L., Luo S., Rouleau C.M., Ivanov I.N., Ji H., Qin Z., Wu Z. *Nanoscale* **2019**, *11*, 8138–8149, doi: 10.1039/C9NR00168A.
78. Sun Y., Jin D., Sun Y., Meng X., Gao Y., Dall'Agnese Y., Chen G., Wang X.F. *J. Mater. Chem. A* **2018**, *6*, 9124–9131, doi: 10.1039/C8TA02706D.
79. Xu F., Li Z., Fan D., Zhao C., Yang X. *Surf. Interfaces* **2024**, *51*, 104658, doi: 10.1016/j.surfin.2024.104658.
80. Huang K., Li C., Zhang X., Wang L., Wang W., Meng X. *Green Energy Environ.* **2023**, *8*, 233–245, doi: 10.1016/ J.GEE.2021.03.011.
81. Sherryna A., Tahir M., Zakaria Z.Y. *Int. J. Hydrogen Energy* **2024**, *51*, 1511–1531, doi: 10.1016/j.ijhydene.2023.09.234.
82. Lee D.E., Jyothirmai M. V., Mameda N., Jo W.K., Tonda S. *Appl. Surf. Sci.* **2024**, *669*, 160516, doi: 10.1016/J.APSUSC. 2024.160516.
83. Wang Q., Chen F., Cai M., Chen J., Jiang Y., Cheng Q., Song Z., Bai J. qi, Wei Y., Sun S. *Catal. Today* **2024**, *435*, 114719, doi: 10.1016/J.CATTOD.2024.114719.
84. Zhou H., Tian J., Wang R., Zhan D., Liu P., Chen R., Huang Y., Liu Z., Han C. *Ceram. Int.* **2023**, *49*, 13042–13049, doi: 10.1016/J.CERAMINT.2022.12.178.
85. Liu D., Li C., Ge J., Zhao C., Zhao Q., Zhang F., Ni T., Wu W. *Appl. Surf. Sci.* **2022**, *579*, 152180, doi: 10.1016/ J.APSUSC.2021.152180.
86. Wong K.J., Foo J.J., Siang T.J., Khoo V., Ong W.J. *Glob. Challenges* **2024**, *8*, 2300235, doi: 10.1002/gch2.202300235.

87. Sun L., Qi Y., Jia C.J., Jin Z., Fan W. *Nanoscale* **2014**, *6*, 2649–2659, doi: 10.1039/C3NR06104C.
88. Kozlova E.A., Parmon V.N. *Russ. Chem. Rev.* **2017**, *86*, 870, doi: 10.1070/RCR4739.
89. Erwin S.C., Zu L., Haftel M.I., Efros A.L., Kennedy T.A., Norris D.J. *Nature* **2005**, *436*, 91–94, doi: 10.1038/nature03832.
90. Rasouli K., Rasouli J., Mohtaram M.S., Sabbaghi S., Kamyab H., Moradi H., Chelliapan S. *J. Clean. Prod.* **2023**, *419*, 138181, doi: 10.1016/J.JCLEPRO.2023.138181.
91. Bolisetty S., Peydayesh M., Mezzenga R. *Chem. Soc. Rev.* **2019**, *48*, 463–487, doi: 10.1039/C8CS00493E.
92. Wu Y., Liu Y., Kamyab H., Rajasimman M., Rajamohan N., Ngo G.H., Xia C. *Environ. Res.* **2023**, *232*, 116363, doi: 10.1016/J.ENVRES.2023.116363.
93. Budnikova Y.B., Vasilyeva M.S., Lukiyanchuk I.V. *ChemChemTech* **2025**, *68*, 79–87, doi: 10.6060/ivkkt.20256802.7072.
94. Hao N.H., Lan P.T., Giang N.T.K., Chau C.H.M., Ha N.T.T. *ChemChemTech* **2025**, *68*, 25–32, doi: 10.6060/ivkkt.20256804.7128.
95. Nasri M.S.I., Samsudin M.F.R., Tahir A.A., Sufian S. *Energies* **2022**, *15*, 955, doi: 10.3390/EN15030955.
96. Li C., Kan C., Meng X., Liu M., Shang Q., Yang Y., Wang Y., Cui X. *Nanomaterials* **2022**, *12*, 4015, doi: 10.3390/NANO12224015/S1.
97. Zhang H., Xu J., Yuan Y., Guo Y., Tan X., Wang H., Hu X., Tang C. *Sep. Purif. Technol.* **2024**, *330*, 125520, doi: 10.1016/J.SEPPUR.2023.125520.
98. Jin D., Lv Y., He D., Zhang D., Liu Y., Zhang T., Cheng F., Zhang Y. nan, Sun J., Qu J. *Chemosphere* **2022**, *308*, 136461, doi: 10.1016/J.CHEMOSPHERE.2022.136461.
99. Abbas H.A., Abbas K.K., Abdulkadhim Al-Ghaban A.M.H. *Results Chem.* **2025**, *13*, 101934, doi: 10.1016/J.RECHEM.2024.101934.
100. Xu R., Wei G., Xie Z., Diao S., Wen J., Tang T., Jiang L., Li M., Hu G. *J. Alloys Compd.* **2024**, *970*, 172656, doi: 10.1016/J.JALLCOM.2023.172656.
101. Zhang J., Shao C., Lei Z., Li Y., Bai H., Zhang L., Ren G., Wang X. *J. Mater. Sci. Technol.* **2024**, *194*, 124–137, doi: 10.1016/J.JMST.2024.02.005.
102. Saafie N., Sufian S., Mufti N., Samsudin M.F.R. *J. Mater. Sci. Mater. Electron.* **2025**, *36*, 1–15, doi: 10.1007/s10854-025-14395-w.
103. Ya Z., Wang Q., Cai J., Wang P., Jiang X., Cai Z., Xiang S., Wang T., Cai D. *J. Environ. Sci.* **2024**, *137*, 258–270, doi: 10.1016/J.JES.2022.10.049.
104. Liu W., Sun M., Ding Z., Gao B., Ding W. *J. Alloys Compd.* **2021**, *877*, 160223, doi: 10.1016/J.JALLCOM.2021.160223.
105. Qiao L. Le, Zhang F.J., Kai C.M., Liu C., Wang Y.R., Oh W.C. *J. Korean Ceram. Soc.* **2023**, *60*, 790–797, doi: 10.1007/s43207-022-00269-y.
106. Nasri M.S.I., Samsudin M.F.R., Tahir A.A., Sufian S. *Energies* **2022**, *15*, 955, doi: 10.3390/EN15030955.
107. Zhou W., Yu B., Zhu J., Li K., Tian S. *New J. Chem.* **2022**, *46*, 14793–14804, doi: 10.1039/D2NJ02658A.
108. Huang N.Y., Chen D., Zheng Y.T., Xu Q. *Chem. – A Eur. J.* **2025**, *31*, e02207, doi: 10.1002/CHEM.202502207.
109. Dhiman P., Sharma J., Kumar A., Sharma G., Dawi E.A. *Chem. Eng. Res. Des.* **2024**, *203*, 263–279, doi: 10.1016/J.CHERD.2024.01.034.
110. Li X., Bai Y., Shi X., Huang J., Zhang K., Wang R., Ye L. *Appl. Surf. Sci.* **2021**, *546*, 149111, doi: 10.1016/J.APSUSC.2021.149111.
111. Zhong R., Liang Y., Huang F., Liang S., Liu S. *Chinese J. Catal.* **2023**, *53*, 109–122, doi: 10.1016/S1872-2067(23)64513-9.
112. Hu J., Ding J., Zhong Q. *J. Colloid Interface Sci.* **2021**, *582*, 647–657, doi: 10.1016/J.JCIS.2020.08.047.
113. Madi M., Tahir M., Zakaria Z.Y. *J. CO2 Util.* **2022**, *65*, 102238, doi: 10.1016/J.JCOU.2022.102238.
114. Tang Q., Sun Z., Deng S., Wang H., Wu Z. *J. Colloid Interface Sci.* **2020**, *564*, 406–417, doi: 10.1016/j.jcis.2019.12.091.
115. Yang C., Tan Q., Li Q., Zhou J., Fan J., Li B., Sun J., Lv K. *Appl. Catal. B Environ. Energy* **2020**, *268*, 118738, doi: 10.1016/J.APCATB.2020.118738.
116. Ye M., Wang X., Liu E., Ye J., Wang D. *ChemSusChem* **2018**, *11*, 1606–1611, doi: 10.1002/CSSC.201800083.

Received 27.10.2025
Accepted 17.11.2025